Study on the stability of surrounding rock in the underground space of coastal reef limestone

Xiaoqing Wei [1, 2, a], Yi Luo [1, 2, b], Shangyuan Chen [3, c], Xinping Li [1, 2, d], Mingju Mao [1, 2, e], Da Mei [1, 2, f]

[1] Sanya Science and Education Innovation Park, Wuhan University of Technology, Sanya 572024, China;

[2] School of Civil Engineering and Architecture, Wuhan University of Technology, Wuhan 430070, China;

[3] Naval research institute, Beijing 100000, China.

[a] xqwei@whut.edu.cn, [b] yluo@whut.edu.cn, [c] ahsscsy@126.com, [d] xinpingli@whut.edu.cn, [e] 348446@whut.edu.cn, [f] 1327159887@qq.com

Abstract. To analyze the stability of the surrounding rock of the underground space of reef limestone. This paper uses COMSOL Multiphysics multi-physics finite element analysis software to study the stable evolution law of the surrounding rock of the underground space of coastal reef limestone. Based on the homogeneous body hypothesis, the influence of the thickness of the side cover and the scale of the cave on the deformation of the surrounding rock of the underground space of reef limestone is analyzed. The study shows that the development of the cave causes the displacement of the surrounding rock, the settlement of the upper part, and the horizontal displacement of the lower part. The deformation peak is positively correlated with the thickness of the side cover and the diameter of the cave. Adjusting these parameters can help control the deformation. Monitoring the displacement around the cave is very important for evaluating the deformation state of the surrounding rock.

Keywords: Underground space; Deformation field; Deformation monitoring.

1. Introduction

In recent years, most of the research results in the field of marine underground space development are based on engineering projects such as submarine tunnels and submarine mining, but there are few studies on the development of underground space on offshore islands[1]. Offshore islands have relatively unique topography and geological conditions. The development and construction conditions of underground space in the area close to the seaward slope below sea level are quite different from those of previous marine underground projects. Conducting research on the surrounding rock stability of underground space in this area is of great significance for determining the development boundary of underground space on offshore islands and maximizing the scale of underground space development.

The stability of surrounding rock in marine underground space is a typical fluid-solid coupling problem. Many scholars have conducted research on the stability of surrounding rock under the action of seepage. Based on the relative stiffness method proposed by Einstein and Schwartz, Antoni Bobet[2-3] studied the stress and deformation characteristics of tunnel surrounding rocks and linings under water-bearing conditions through analytical models. Liu et al.[4] introduced the stress adjustment coefficient and further advanced the research by considering the influence of stress redistribution in the elastic zone caused by plastic deformation of the surrounding rock. Rong et al.[5] applied the theory of elastoplastic damage mechanics to derive a theoretical solution to the stability of tunnel surrounding rock under the influence of groundwater seepage. Shen et al.[6] proposed a formula for calculating the safe burial depth of river-crossing tunnels by establishing a differential equation. Wang et al.[7] derived the elastic-plastic analytical solution of the surrounding

rock of upper and lower circular tunnels under water blocking and drainage limiting conditions. Based on the assumption of constant total stress, Zhu[8] derived an analytical solution for the seepage field response of the tunnel surrounding rock under the action of constant dynamic water level, analyzed the water and soil pressure response of the underwater tunnel, and provided a theoretical basis and technical guidance for submarine engineering construction.

Since there are few marine underground projects and insufficient actual engineering data, numerical simulation can also provide a theoretical basis for the construction of marine underground space. Therefore, in the field of numerical simulation research, Li[9] used PLAXIS 3D to perform numerical simulation of excavation and removal of support for the auxiliary working shaft of tunnel construction, taking the Changxing Island Cross-River Tunnel Project as the background. Sun et al.[10] established a three-dimensional numerical model of the Gaoyatou Tunnel to study the development trend of the displacement of the surrounding rock under seepage conditions, and found that the deformation considering seepage was closer to the monitoring value than that under no seepage conditions. Li et al.[11] used the FLAC 3D software platform to study the influence of water seepage on tunnel construction under different groundwater levels and different drainage conditions, and verified that the design of the tunnel support structure needs to consider the effect of seepage.

The coastal underground space project involved in this study is located in the continental slope area of the South China Sea. Unlike existing marine underground projects, the existing geological conditions can be roughly divided into sedimentary layers, weathering layers, and bedrock layers from top to bottom, and the bedrock layer is the main surrounding rock of the underground project[12]. However, the thickness of the reefs on the South China Sea islands is between 800-1300m[13]. Therefore, the coastal underground space development on the South China Sea islands generally cannot reach the bedrock layer, and the surrounding rock will be mainly reef limestone[14]. The physical and mechanical properties of reef limestone are significantly different from those of terrigenous rock bodies[15-16]. Based on this, this paper intends to obtain the changing laws of the surrounding rock of the coastal reef limestone underground space through numerical simulation methods. It provides a theoretical basis for the development boundary of the underground space of offshore islands and maximizing the scale of underground space development.

2. Numerical simulation methods

2.1 Project Overview

For marine underground projects, the relationship between rock and soil, water and artificial structures is the basis for studying the stability of the surrounding rock of marine underground space projects[17-19]. The distribution characteristics of the seaside underground space involved in this paper are different from those of previous marine underground space projects. Due to the limitation of being surrounded by water, the space available for development at the same buried depth is limited. Therefore, the seaside underground space should be as close to the seaward slope as possible to improve the efficiency of space utilization. To simplify the analysis, it is assumed that the cross section of the seaside underground space is circular, and the axis is parallel to the coastline. A generalized engineering model is established for analysis.

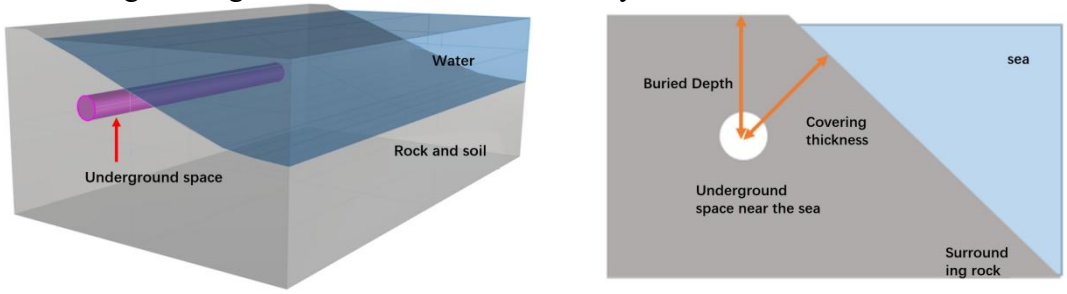

Fig. 1 Generalized model of coastal underground space

Fig. 2 Values of burial depth and cover thickness

As shown in Figure 1, on the whole, the rock and soil, water bodies, and underground space of the coastal underground space have the characteristics of horizontal distribution in space. At the same time, the underground space is close to the interface between the rock and soil and water bodies, and the three have significant mutual influences.

The location of the seaside underground space is determined by two parameters: the thickness of the cover layer and the burial depth. The burial depth refers to the vertical distance from the center of the cavern to the surface of the site, reflecting the initial geostress and hydrostatic pressure. The thickness of the cover layer refers to the vertical distance from the center of the cavern to the slope of the seaward slope, which affects the surrounding rock stress and seepage force after excavation. These two parameters not only determine the spatial position of the cavern, but also show the relative position relationship between the cavern and the seaward slope. The values of the burial depth and the cover layer thickness are shown in Figure 2.

In summary, considering the current situation that specific data on island and reef geological conditions are difficult to obtain and actual engineering data are lacking, the thickness of the lateral covering layer and the size of the cavern are selected as the main influencing factors for analysis in the subsequent study of the surrounding rock stability of the underground space of coastal reef limestone.

2.2 Software underlying equations

This paper uses COMSOL Multiphysics multi-physics finite element analysis software to carry out research. This software has powerful multi-field coupling calculation functions and has been widely used in the field of geotechnical engineering. The research in this chapter mainly involves the "solid mechanics", "Darcy's law" physical fields and "porous elasticity" multi-physics fields in this software. Generally speaking, the research problems involving time variables in COMSOL Multiphysics software are called transient research, and the opposite is called steady-state research. The research in this chapter is mainly steady-state research.

The solid mechanics physics module can calculate and analyze the displacement, stress, and strain of two-dimensional, three-dimensional, or axisymmetric bodies under load. When solving steady-state problems, the underlying equations of the software are as follows:

$$-\nabla \cdot \boldsymbol{\sigma} = \boldsymbol{f} \tag{1}$$

In formula (1), σ is stress and is the Laplace operator.

The Darcy's law physics field can calculate and analyze the pore pressure distribution, flow velocity and other results when the fluid flow in an object conforms to Darcy's law. The underlying equation of the software is as follows:

$$\begin{cases} \nabla \cdot (\rho \boldsymbol{u}) = Q_m \\ \boldsymbol{u} = -\dfrac{K}{\rho g}(\nabla p + \rho g \nabla D) \end{cases} \tag{2}$$

In formula (2), ρ is the fluid density, $\boldsymbol{u}$ is the Darcy velocity, Q_m is a mass source term with the unit of kg/(m^3·s), K is the permeability coefficient (also known as hydraulic conductivity in the software), p is the water pressure, g is the gravitational acceleration, and D is the elevation.

The poroelastic multi-physics module generally refers to the fluid-solid coupling (Biot consolidation) theory[20], which can realize the direct coupling of the solid mechanics physics field and the Darcy's law physics field in the established research model. In simple terms, its implementation method is to take the pore pressure in the Darcy's law physics field as a load into the solid mechanics physics field. The volume strain in the solid mechanics physics field will directly affect the calculation of the mass source term in the Darcy's law physics field. The underlying equation is as follows:

$$\rho_f S\frac{\partial p}{\partial t}+\nabla\bullet\left(\rho_f \boldsymbol{u}\right)=-\rho_f\alpha_B\frac{\partial}{\partial t}\varepsilon_{vol} \quad (3)$$

$$\rho\frac{\partial^2 \boldsymbol{u}}{\partial t^2}=\nabla_x\sigma+\boldsymbol{f}_V \quad (4)$$

$$S=\frac{\varepsilon_p}{K_f}+\frac{\alpha_B-\varepsilon_p}{K_S} \quad (5)$$

$$\sigma=\mathbf{C}\varepsilon-\alpha_B p\mathbf{I} \quad (6)$$

In formula (3), ρ_f is the fluid density, S is the water storage coefficient, ρ is the solid material density, p is the pore pressure in the solid, and $\boldsymbol{u}$ is the Darcy velocity of the fluid; α_B is the biot coefficient, ε_{vol} is the unit strain change, $\boldsymbol{\sigma}$ is the stress, $\boldsymbol{f}_V$ is the body load, ε_p is the material porosity, K_f is the fluid compressibility, Ks is the solid elastic coefficient, and ε is the strain.

It can be seen from the underlying equations of the above software that during direct coupling calculations, changes in the porosity ε_p will cause changes in the water storage coefficient S. The water storage coefficient S is affected by the joint influence of the fluid and the solid. The stress in the area is determined by the strain and the fluid pressure, thereby realizing direct fluid-solid coupling calculation research.

2.3 Parametric Modeling

The model is based on the following assumptions: a two-dimensional model is established in the area near the seaward slope of the island axis; the construction site is assumed to be a saturated homogeneous body in which water seepage conforms to Darcy's law; the ocean dynamic condition load is ignored, and seawater acts on the seaward slope in the form of hydrostatic pressure; construction disturbances such as explosions and tunnel excavation are ignored.

This study conducts modeling and analysis on coastal underground space. Combined with Section 1.1, the numerical model overview of coastal underground space is shown in Figure 1-3.

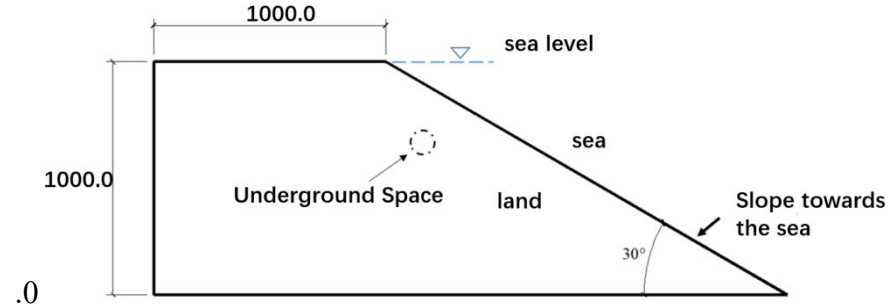

Fig. 3 Overview of the numerical model of Linhai underground space

As shown in Figure 3, the numerical model established this time is a right-angled trapezoid as a whole, with a top width of 1000m, the top surface of the model is 0m at sea level, a depth of 1000m, and the foot of the seaward slope is 30°. The cross-sectional shape of the underground space to be analyzed is circular, and its location is on the ocean side of the top of the seaward slope. Since the research process involves calculations of working conditions with different diameters, different burial depths, and different cover thicknesses, the geometric features of the circular cavern are parameterized in the model to facilitate modeling research.

A rectangular coordinate system is established with the top of the seaward slope as the coordinate base point (0,0), the horizontal direction from the land to the ocean as the X-axis, and the gravity direction as the Y-axis. At this time, the coordinates of the center of the circular cavern in this coordinate system are marked as (x, y), the diameter of the cavern is a m, the distance between the center of the cavern and the seaward slope (i.e., the thickness of the side covering layer) is recorded as $l=(n*a)$ m, and the foot of the seaward slope is recorded as θ. At this time, in order to facilitate the analysis of different cavern scale working conditions later, referring to previous underground projects, the ratio of the cavern diameter to the side covering layer thickness is taken

as the side covering thickness coefficient, and its value is recorded as n. In the specific research process, the parameters a、θ、n and the burial depth d are all known parameters, so the values of the circular cavern coordinates (x, y) can be obtained according to the geometric relationship shown in Figure 1-4.

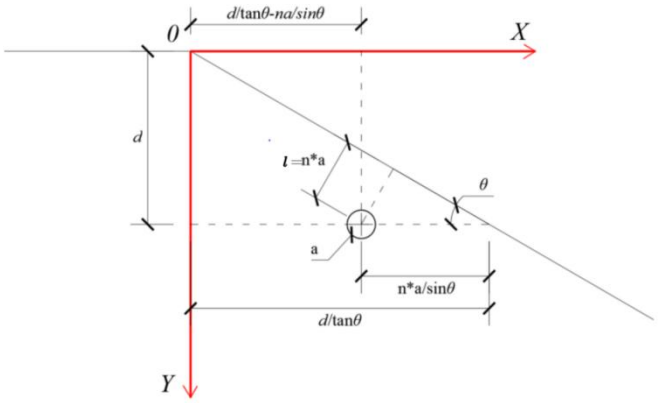

Fig. 4 Analysis of the center coordinates of the circular cavern in the seaside underground space

As shown in Figure 4, the coordinates (x, y) of the center point of the underground cavern are as shown in formula (7).

$$\begin{cases} x = d / \tan\theta - na / \sin\theta \\ y = d \end{cases} \tag{7}$$

At this time, by inputting different values of parameters a, θ, n, and d, the geometric model under different working conditions can be automatically obtained, thereby realizing rapid calculation and analysis.

The boundary condition settings of this model are shown in Figure 1-5.

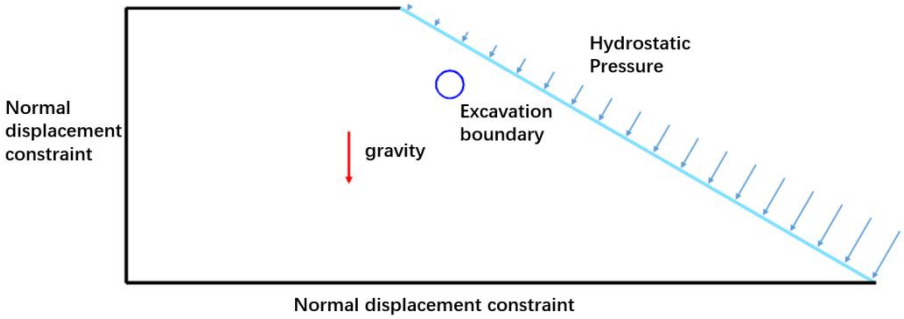

Fig. 5 Boundary conditions of the numerical model

As shown in Figure 5, the bottom and left boundaries of the numerical model are normal displacement constraint boundaries, the cavern contour is the excavation boundary, and the right sea slope boundary is the hydrostatic pressure boundary. The solid field and seepage field in the model both take into account the influence of gravity. The commonly used method for determining the water pressure value in submarine tunnel calculations is referenced[24].

The Hoek-Brown constitutive model is used for rock mass material constitutive model. The original Hoek-Brown failure criterion stipulates:

$$\sigma_1 = \sigma_3 + \sqrt{m\sigma_{cs}\sigma_3 + s\sigma_{cs}^2} \tag{8}$$

In formula (8), $\sigma_1 \geq \sigma_2 \geq \sigma_3$ is the principal stress at failure, σ_{cs} is the uniaxial compressive strength of intact rock, and m and s are material parameters. The material parameters in the numerical model are shown in Table 1. The numerical model mesh is divided using free triangle mesh. Considering the calculation amount and calculation accuracy, the division parameters are shown in Table 2. The mesh around the cave is encrypted, and the final model mesh division is shown in Figure 6.

Table 1 Numerical model material parameters

Density g·cm^3	Porosity %	Young's modulus GPa	Poisson's ratio	Permeability coefficient cm/s	Compressive strength MPa	tensile strength MPa	Parameter m	Parameter s
1.59	41	5.5	0.25	3.94×10-4	10	1.2	5	0.5

Table 2 Numerical model meshing parameters

Maximum unit	Minimum unit	Maximum unit growth rate	Curvature Factor	Narrow area resolution
1.69	35	5.5	0.25	10

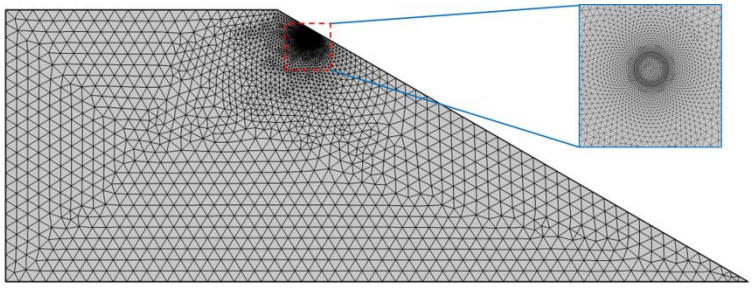

Fig. 6 Numerical model mesh division

This numerical model uses steady-state research for calculation and analysis, and a single model is solved in two steps: Step 1, perform fluid-solid coupling calculation on the model when no cavern excavation is performed to obtain the initial geostress field and pressure field data; Step 2, call the calculation results of Step 1, balance the geostress by applying prestress, and remove the excavation area in this step, set the excavation boundary to the seepage boundary with a water pressure of 0, and thus calculate the final result.

3. Deformation law of surrounding rock in underground space of coastal reef limestone

3.1 Influence of lateral cover thickness on surrounding rock deformation

This section mainly analyzes the deformation of the surrounding rock in the underground space when the burial depth (d) is 100m, the cavern diameter (a) is 10m, and the side cover thickness coefficient n is 1.0, 2.0, 3.0, 4.0, and 5.0 respectively.

The horizontal displacement of the surrounding rock in the underground space of coastal reef limestone under different side cover thickness conditions is shown in Figure 7.

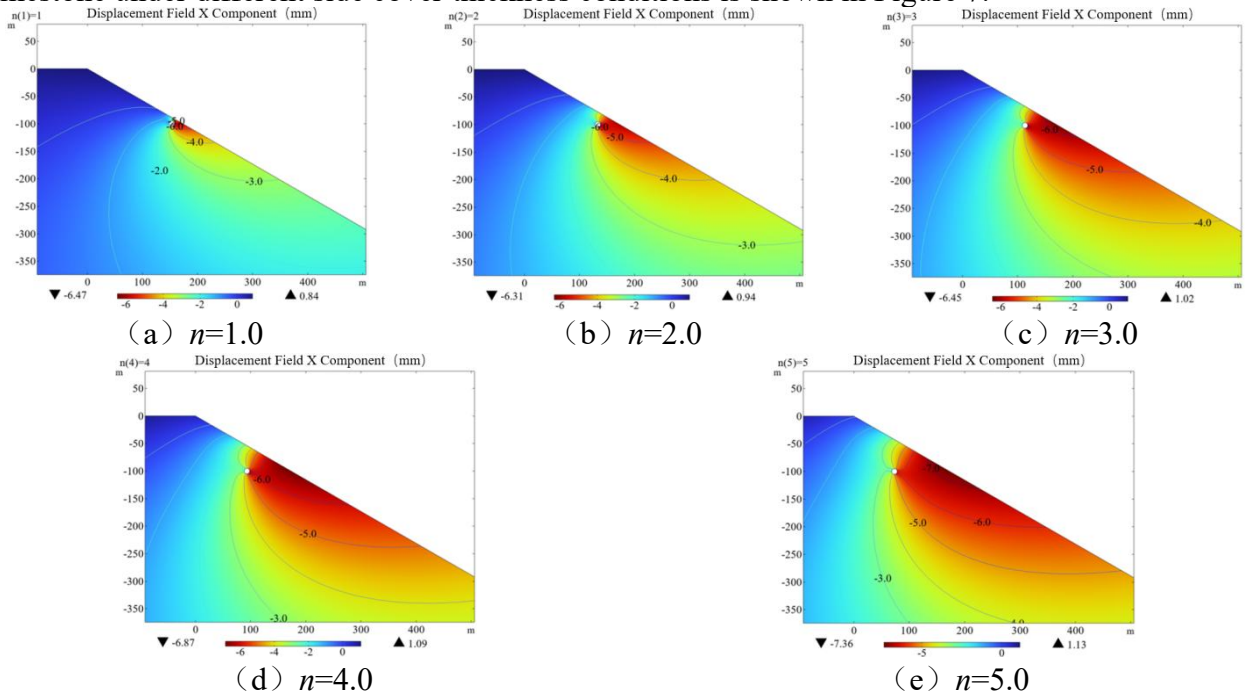

（a）n=1.0 （b）n=2.0 （c）n=3.0

（d）n=4.0 （e）n=5.0

Figure 7 Cloud diagram of horizontal displacement of surrounding rock under different side

cover thickness

As shown in Figure 7, the peak value of the horizontal displacement of the surrounding rock first decreases and then increases with the increase of the side cover thickness coefficient *n*. It is the smallest when *n*=2, which is 6.31 mm, and the largest when *n*=5, which is 7.36 mm. It mainly affects the area on the right side of the vertical line between the cavern and the seaward slope. The displacement direction is horizontal to the left, and it has little effect on the top of the slope. The horizontal displacement contour lines are mainly arcs connecting the cavern outline and the seaward slope surface below the cavern burial depth, which is similar to the distribution of the slope sliding zone. The displacement contour lines at the same level continue to move to the left with the increase of *n*, and the area continues to expand.

The vertical displacement of the surrounding rock in the underground space of coastal reef limestone under different side cover thickness conditions is shown in Figure 8.

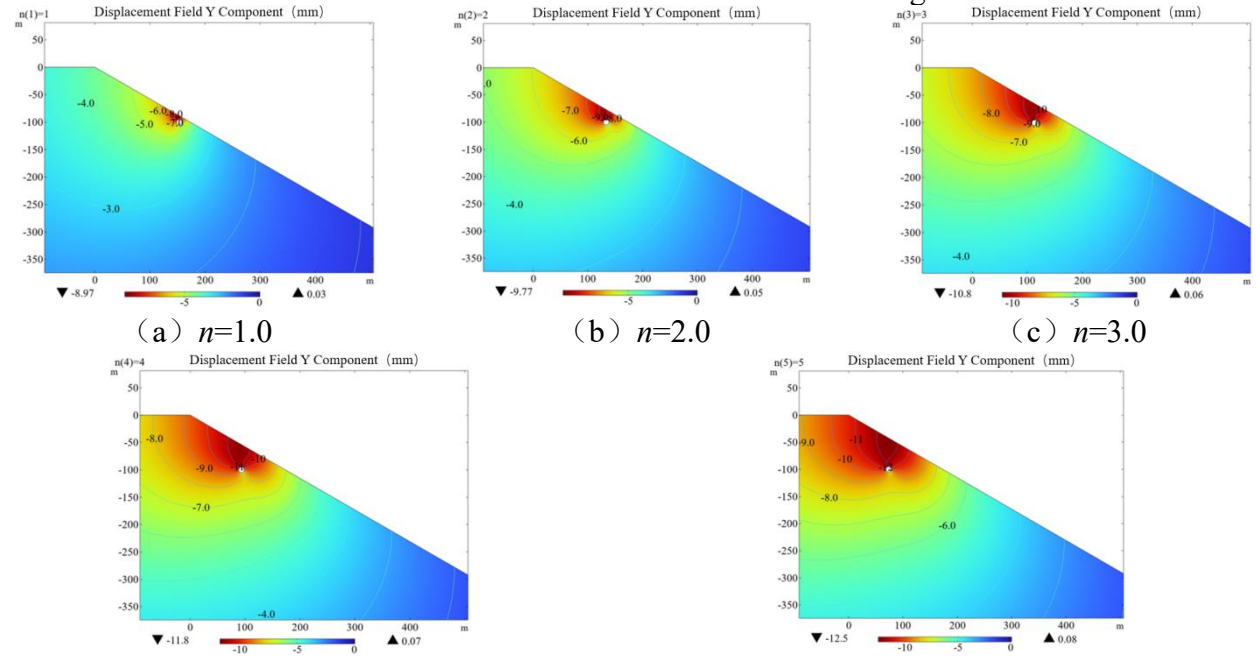

（a）*n*=1.0 （b）*n*=2.0 （c）*n*=3.0

（d）*n*=4.0 （e）*n*=5.0

Fig. 8 Cloud diagram of vertical displacement of surrounding rock under different side cover thickness

As shown in Figure 8, the peak value of the vertical displacement of the surrounding rock increases with the increase of the side cover thickness coefficient *n*. It is the smallest when *n*=1, which is 8.97 mm, and the largest when *n*=5, which is 12.5 mm. It mainly affects the rock strata above the cavern, and the displacement direction is vertically downward, which has a greater impact on the top of the slope. The vertical displacement contour lines are mainly arcs connecting the cavern outline and the seaward slope surface higher than the cavern burial depth and the top of the slope. The displacement contour lines at the same level continue to move downward with the increase of *n*, and the affected area continues to expand.

The overall displacement of the surrounding rock in the underground space of coastal reef limestone under different side cover thickness conditions is shown in Figure 9.

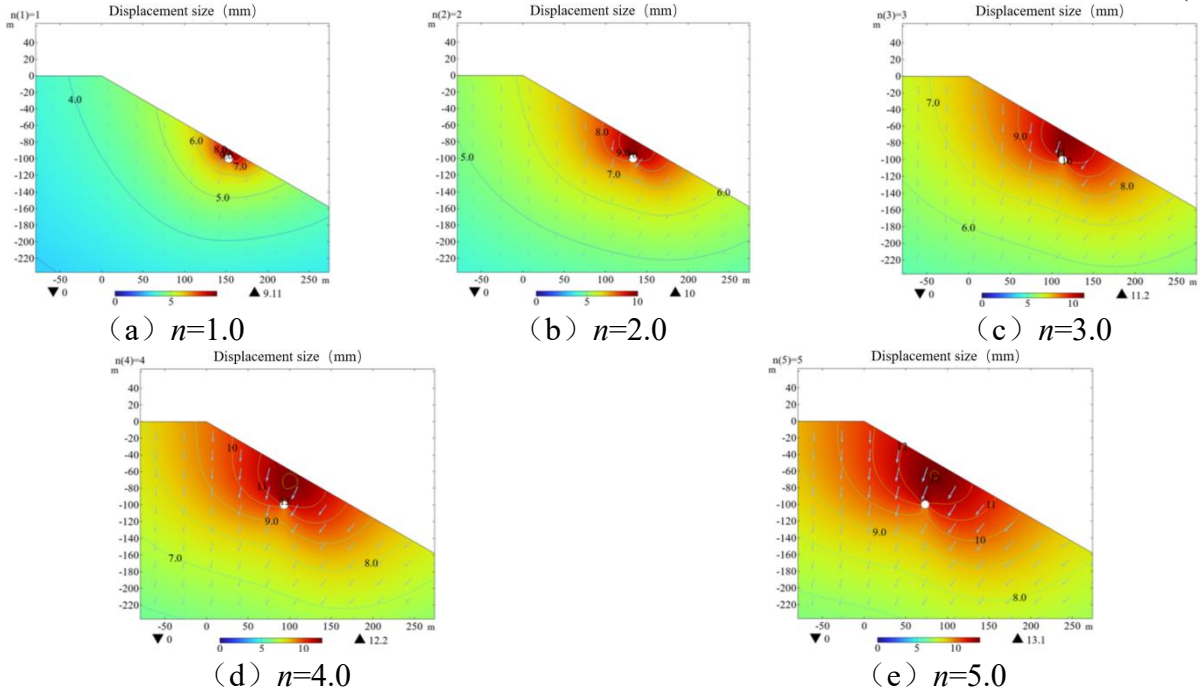

（a）n=1.0 （b）n=2.0 （c）n=3.0

（d）n=4.0 （e）n=5.0

Fig. 9 Cloud diagram of total displacement of surrounding rock under different side cover thickness

As shown in Figure 9, the peak value of the total displacement of the surrounding rock increases with the increase of the side cover thickness coefficient n. It is the smallest when n=1, which is 9.11mm, and the largest when n=5, which is 13.1mm. It mainly affects the area between the underground space and the seaward slope. As can be seen from the arrow representing the displacement direction in the figure, the displacement direction of the surrounding rock is vertical to the slope, deflected toward the underground space, and pointed to the interior of the land. The total displacement contour line is mainly composed of arcs connecting the two sides of the cavern contour and the seaward slope. The contour lines at the same level continue to move downward with the increase of n, and the affected area continues to expand. Combined with the previous text, it can be seen that with the cavern center and the vertical line of the seaward slope as the boundary, the rock displacement in the upper area is mainly settlement, the rock displacement in the lower area is mainly horizontal displacement, and the area near the vertical line is mainly displacement toward the cavern.

In order to study the influence of the side cover thickness on the deformation of the underground space cave, a polar coordinate diagram of the displacement around the cave was drawn as shown in Figure 10. The polar coordinate axis takes the center of the cave as the origin, and the horizontal right direction is 0°.

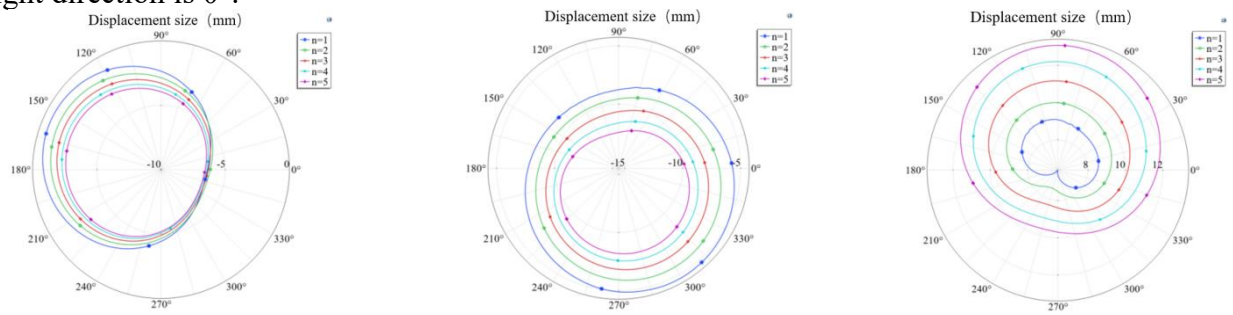

（a）Horizontal displacement （b）Vertical displacement （c）Total displacement

Fig. 10 Polar coordinate diagram of tunnel perimeter displacement under different side covering coefficients

As shown in Figure 10 (a), the horizontal displacement around the cave first decreases and then increases with the side cover thickness coefficient n. The displacement amplitude is the smallest

when n=2, which is 6.31mm, and the largest when n=5, which is 6.66mm. The numerical horizontal displacements are all <0, indicating that the cave is displaced horizontally to the left as a whole. The horizontal displacements on the left and right sides of the cave are quite different, and the vertical displacement amplitude of the right half is greater than that of the left half. The maximum displacement is at about 340°~345° on the cave wall.

As shown in Figure 10 (b), the vertical displacement around the cave increases with the increase of the side cover thickness coefficient n. It is the smallest when n=1, which is 8.97 mm, and the largest when n=5, which is 12.53 mm. The vertical displacements are numerically <0, indicating that the cave is displaced downward as a whole in the vertical direction. The horizontal displacements on the upper and lower sides of the cave are quite different, with the displacement amplitude of the upper half being greater than that of the lower half, and the maximum displacement is at about 105°~118° of the cave wall.

As shown in Figure 10 (c), the total displacement around the cave increases with the increase of the side cover thickness coefficient n. It is the smallest when n=1, which is 9.11 mm, and the largest when n=5, which is 13.05 mm. The total displacement of the cave is quite different between the near sea slope side and the far sea slope side. The displacement amplitude on the near sea slope side is greater than that on the far sea slope side, and the maximum displacement is approximately at the cave wall in the direction of 88°~101°.

3.2 Effect of cavern size on surrounding rock deformation

This section mainly analyzes the deformation of the surrounding rock in the underground space when the cavern diameter (a) is 5m, 10m, 20m and 30m respectively under the conditions of burial depth (d) of 100m and side cover thickness coefficient (n) of 3.

The horizontal displacement of the surrounding rock in the underground space of coastal reef limestone under different cavern sizes is shown in Figure 11.

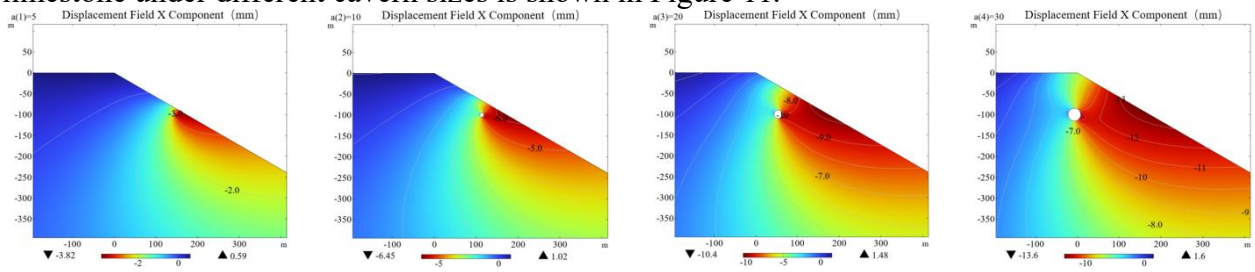

（a）a=5m （b）a=10m （c）a=20m （d）a=30m

Fig. 11 Cloud diagram of horizontal displacement of surrounding rock under different cavern scales

As shown in Figure 11, the amplitude of the horizontal displacement of the surrounding rock increases with the increase of the diameter a of the cavern. It is the smallest when a=5, which is 3.82mm, and the largest when a=30, which is 13.6mm. It mainly affects the area on the right side of the vertical line between the cavern and the seaward slope. The displacement direction is horizontal to the left, and has little impact on the top of the slope. The impact is only greater when the cavern is directly below the top of the slope (a=30m). The horizontal displacement contour lines are mainly arcs connecting the cavern outline and the seaward slope surface. The displacement contour lines at the same level continue to move to the left with the increase of a, and the area continues to expand.

The vertical displacement of the surrounding rock in the underground space of coastal reef limestone under different cavern sizes is shown in Figure 12.

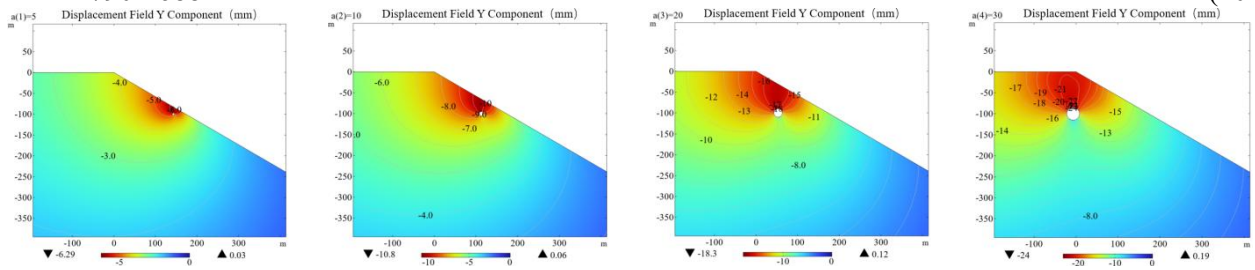

（a）a=5m （b）a=10m （c）a=20m （d）a=30m

Fig. 12 Cloud diagram of vertical displacement of surrounding rock under different cavern sizes

As shown in Figure 12, the amplitude of the vertical displacement of the surrounding rock increases with the increase of the diameter a of the cavern, and is the smallest when a=5, which is 6.29 mm, and the largest when a=30, which is 24 mm; it mainly affects the rock strata overlying the cavern, and the displacement direction is vertically downward, which has a greater impact on the top of the slope; the vertical displacement contour lines are mainly arcs connecting the cavern outline and the seaward slope surface higher than the cavern burial depth and the top of the slope; the displacement contour lines at the same level continue to move downward with the increase of a, and the affected area continues to expand.

The overall displacement of the surrounding rock in the underground space of coastal reef limestone under different cavern sizes is shown in Figure 13.

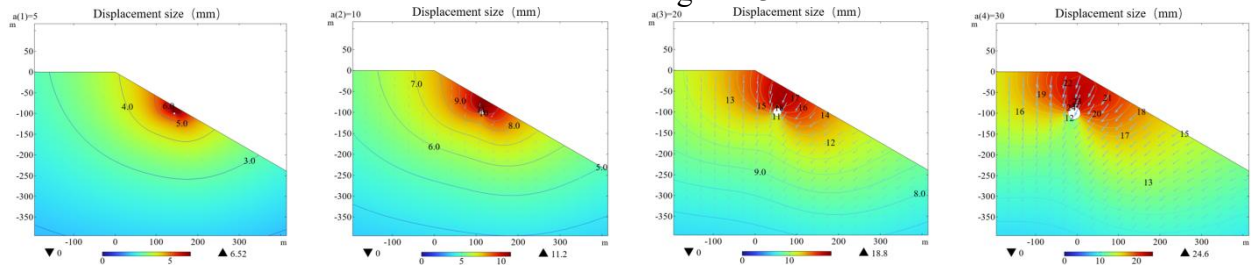

（a）a=5m （b）a=10m （c）a=20m （d）a=30m

Fig. 13 Cloud diagram of total displacement of surrounding rock under different cavern sizes

As shown in Figure 13, the total displacement amplitude of the surrounding rock increases with the increase of the cavern diameter a. It is the smallest when a=5, which is 6.52mm, and the largest when a=30, which is 24.6mm. It mainly affects the area between the underground space and the seaward slope. When the cavern is located directly below the top of the slope, it also has a great impact on the top of the slope. It can be seen from the arrow representing the displacement direction in the figure that the displacement direction of the surrounding rock is vertical to the slope, deflected toward the underground space, and pointing to the interior of the land. The total displacement contour lines are mainly arcs connecting the two sides of the cavern outline and the seaward slope. The contour lines at the same level continue to move downward with the increase of a, and the affected area continues to expand.

The polar coordinate diagram of the displacement around the underground space under different cavern sizes is shown in Figure 14. The polar coordinate axis takes the center of the cavern as the origin, and the horizontal right direction is 0°.

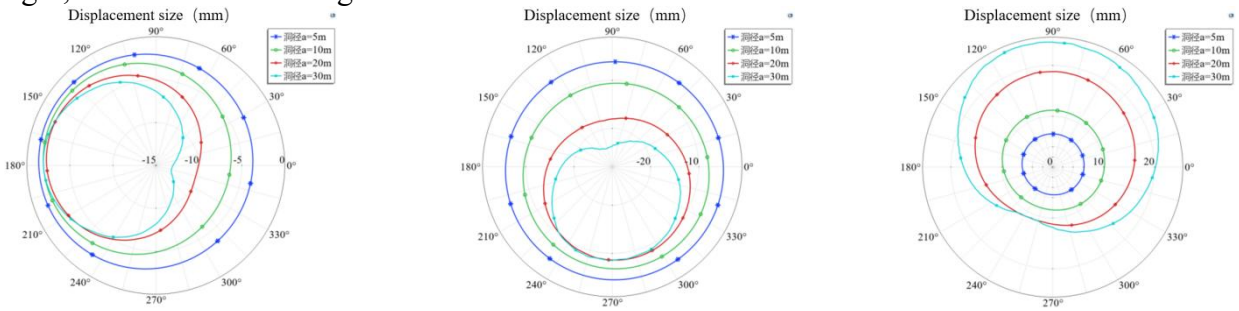

（a）Horizontal displacement （b）Vertical displacement （c）Total displacement

Fig. 14 Polar coordinate diagram of cave displacement at different cave scales

As shown in Figure 14 (a), the peak value of the horizontal displacement around the cave increases with the increase of the diameter *a* of the cave, from 3.82mm to 13.13mm; the horizontal displacement is numerically <0, indicating that the cave is displaced to the left as a whole; the horizontal displacement on the left and right sides of the cave is quite different, the vertical displacement of the right half is greater than that of the left half, and the maximum displacement is approximately at 339°~348° on the cave wall.

As shown in Figure 14 (b), the peak value of the vertical displacement around the cave increases with the increase of the diameter *a* of the cave, from 6.29 mm to 24.05 mm; the vertical displacement is numerically <0, indicating that the cave is displaced downward as a whole in the vertical direction; the horizontal displacement on the upper and lower sides of the cave is quite different, the displacement amplitude of the upper half is greater than that of the lower half, and the maximum displacement is approximately at 100°~120° to the cave wall.

As shown in Figure 14 (c), the peak value of the total displacement around the cave increases with the increase of the cave diameter *a*, from 6.52mm to 24.60mm; the total displacement of the cave is quite different between the near sea slope side and the far sea slope side, the displacement amplitude on the near sea slope side is greater than that on the far sea slope side, and the maximum displacement is approximately at the cave wall in the direction of 94°~100°.

3.3 Deformation change law of surrounding rock

In order to analyze the influence of the thickness of the side cover and the size of the cave on the deformation field of the surrounding rock, the scatter fitting relationship diagrams of each factor and the peak deformation of the cave perimeter and the peak deformation of the seaward slope were drawn respectively.

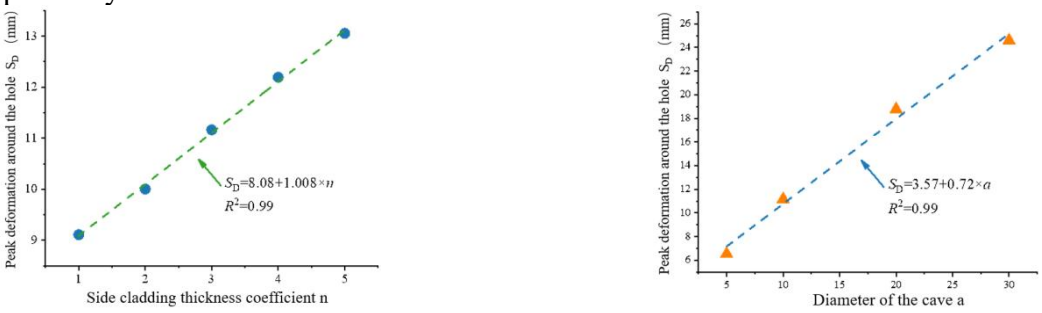

（a）Side cladding thickness factor *n* （b）Diameter of the cave *a*

Fig. 15 Variation of peak deformation around the hole

As shown in Figure 25, the peak value of the tunnel deformation (S_D) shows a good linear positive correlation with the side cover thickness coefficient and the tunnel diameter. The specific relationship is:

$$S_D = 8.08 + 1.008 \times n \left(R^2 = 0.99\right) \quad (9)$$

$$S_D = 3.57 + 0.72 \times a \left(R^2 = 0.99\right) \quad (10)$$

The peak value of cave deformation has a high linear correlation with the side cover thickness coefficient and cave diameter, and the correlation coefficient is 0.99.

From the above, it can be seen that in order to control the peak deformation around the underground space near the sea, measures such as reducing the side covering thickness and the cavern diameter can be taken.

4. Summary

In this paper, COMSOL Multiphysics multi-physics finite element analysis software is used to study the stable evolution law of surrounding rock in the underground space of coastal reef limestone. Based on the homogeneous body assumption, the influence of side cover thickness and cavern scale on the deformation of circular cavern surrounding rock is analyzed, and the following

main conclusions are obtained:

The development of coastal underground space will cause displacement of surrounding rock. With the center of the cavern and the vertical line of the seaward slope as the boundary, the displacement of rock mass in the upper area is mainly settlement, the displacement of rock mass in the lower area is mainly horizontal displacement, and the displacement near the vertical line is mainly toward the cavern. In general, the peak value of cavern deformation shows a good linear positive correlation with the side cover thickness coefficient and cavern diameter. Therefore, for the deformation control of coastal underground space engineering, it is possible to adjust the side cover thickness coefficient and cavern diameter; the research results also suggest that monitoring the displacement of caverns is helpful to evaluate the deformation state of surrounding rock in underground space.

Acknowledgment

The authors gratefully acknowledge the National Key R&D Program of China (No.2021YFC3100801), the PhD Scientific Research and Innovation Foundation of Sanya Yazhou Bay Science and Technology City (HSPHDSRF-2022-03-009) and the National Natural Science Foundation of China (No. 51779197).

References

[1] Benardos A, Athanasiadis I, Katsoulakos N. Modern earth sheltered constructions: A paradigm of green engineering. Tunnelling and Underground Space Technology, 2014, 41: 46-52.

[2] A. Bobet. Effect of pore water pressure on tunnel support during static and seismic loading. Tunnelling and Underground Space Technology, 2003, 18(4): 377-393.

[3] Antonio Bobet. Analytical Solutions for Shallow Tunnels in Saturated Ground. Journal of Engineering Mechanics, 2001, 127(12): 1258-1266.

[4] Liu Cheng-xue, Yang Lin-de, Li Peng. elastic-plastic analytical solution of deep buried circle tunnel considering stress redistribution. Engineering Mechanics, 2009, 26(02): 16-20.

[5] Rong Chuanxin, Cheng Hua. stability analysis of rocks around tunnel with ground water permeation . Chinese Journal of Rock Mechanics and Engineering, 2004, (05): 741-744.

[6] Shen Lin-chong，ZHONG Xiao-chun，QIN Jian-she， et al. Determination of minimum thickness of overburden layer for shield tunnel through Qiantang River. Rock and Soil Mechanies, 2011, 32(1): 111-115.

[7] Wang Xiuying, TAN Zhongsheng, Wang Mengshu, et al. Analysis of mechanical character of surrounding rock with controlled drainage in mountain tunnels. Rock and Soil Mechanies, 2008, 29(1): 75-80.

[8] Zhu Chengwei. Study on Water and Soil Pressure ResponseofSubaqueous Tunnels under Static and Dynamic Water Level .Zhejiang: Zhejiang University, 2020

[9] Li Weitao. Simulation and analysis of deep foundation pit construction of shield working shaft in Shanghai Yuejiang Tunnel . Chinese Journal of Geotechnical Engineering, 2008, 30(S1): 54-58.

[10] Sun qi,Zhang xiangdong,Han peng. Numerical simulation on the effects of seepage on stability for high cliff tunnel. journal of water resources and water engineering, 2011, 22(01): 55-57, 62.

[11] Li Jianbo,Chen Jianyun,Li Jing. Coupled Fluid-Mechanical Analysis of Settlement andStability of Subway Tunnel . Journal of Disaster Prevention and Mitigation Engineering, 2008, (04): 441-446.

[12] Xie H, Zhao J W, Zhou H W, et al. Secondary utilizations and perspectives of mined underground space. Tunnelling and Underground Space Technology, 2020, 96: 103129.

[13] Wang Zhenfeng, Zhang Daojun, Liu Xinyu, et al. Magnetostratigraphy and 230 Th dating of Pleistocene biogenic reefs in XK-1 borehole from Xisha Islands, South China Sea. Chinese Journal of Geophysics, 2017, 60(3): 1027-1038.

[14] Wu Jing, Fu Hao, Zhang Lewen, et al. Stability analysis of surrounding rock in underground chamber excavation of coral reef limestone. Rock Mechanics and Rock Engineering, 2022, 55(8): 4717-4742.

[15] Luo Yi, Li Yueying, Lin Hui, et al. Impact-induced fragmentation of coral reef limestone based on fractal theory. Marine Geophysical Research, 2024, 45(1): 7.

[16] Li Lihui, Li Chenglong, Huang Beixiu, et al. Meso-mechanical anisotropy and fracture evolution of reef limestones from the Maldives Islands and the South China Sea. Journal of Rock Mechanics and Geotechnical Engineering, 2023, 15(12): 3173-3187.

[17] Zhang Yuting, Zuo Dianjun, Pei Wwenbin, et al. Stability analysis of soft soil foundation excavation of underground station in coastal area of Tianjin. Applied Mechanics and Materials, 2014, 501: 1761-1765.

[18] Zhao Kai, Zhu Shengdong, Bai Xiaoxiao, et al. Seismic response of immersed tunnel in liquefiable seabed considering ocean environmental loads. Tunnelling and Underground Space Technology, 2021, 115: 104066.

[19] Zhang X Y, Zhang L W, Wu J, et al. Tunnel stability analysis of coral reef limestone stratum in ocean engineering. Ocean Engineering, 2022, 265: 112636.

[20] Biot,Maurice,A.. General Theory of Three-Dimensional Consolidation. Journal of Applied Physics, 1941, 12(2): 155-164.